Available online at www.sciencedirect.com
ScienceDirect
Journal of Solid State Chemistry 181 (2008) 664–672
JOURNAL OF SOLID STATE CHEMISTRY
www.elsevier.com/locate/jssc

Rapid Communication

Formation of Co^{3+} octahedra and tetrahedra in $YBaCo_4O_{8.1}$

O. Chmaissem[a,b,*], H. Zheng[a], A. Huq[c], P.W. Stephens[d], J.F. Mitchell[a]

[a] *Materials Science Division, Argonne National Laboratory, Argonne, IL 60439, USA*
[b] *Department of Physics, Northern Illinois University, DeKalb, IL 60115, USA*
[c] *Neutron Scattering Science Division, Spallation Neutron Source, P.O. Box 2008, MS 6475, Oak Ridge, TN 37831, USA*
[d] *Department of Physics and Astronomy, Stony Brook University, Stony Brook, NY 11794-3800, USA*

Received 11 September 2007; received in revised form 11 December 2007; accepted 12 December 2007
Available online 25 December 2007

Abstract

High-resolution neutron and synchrotron X-ray powder diffraction experiments were performed, at 300 and 10 K, for the determination of the structure of $YBaCo_4O_{8.1}$, which was prepared by controlled oxidation of the Kagomé lattice compound $YBaCo_4O_7$. Our diffraction data demonstrate that $YBaCo_4O_{8.1}$ crystallizes in the orthorhombic $Pbc2_1$ space group with the formation of a large superstructure ($a = 12.790$ Å, $b = 10.845$ Å, $c = 10.149$ Å), with respect to the parent trigonal $YBaCo_4O_7$ material. The Co ions occupy both corner-sharing tetrahedral and edge-sharing octahedral sites, in contrast to $YBaCo_4O_7$, which has only corner-sharing tetrahedra. The octahedral sites form by the addition of two extra oxygen atoms and the drastic displacements of some of the original O atoms relative to the parent. The edge-sharing octahedra form isolated zigzag chains parallel to the *c*-axis linked to one another via tetrahedra. While found in a few phosphates, silicates and germanates, this motif appears unique to $YBaCo_4O_{8.1}$ among mixed-metal oxides. No structural phase transition or long range antiferromagnetic ordering are observed at 10 K.
© 2008 Elsevier Inc. All rights reserved.

Keywords: $YBaCo_4O_7$; $YBaCo_4O_8$; $RBaCo_4O_7$; $REBaCo_4O_7$; Kagomé lattice; Triangular lattice; Neutron diffraction; Synchrotron X-ray diffraction; Structure determination; Co^{3+} octahedra; Zigzag chains; Edge sharing Co octahedra

1. Introduction

In recent years, cobaltites have been at the center of intense research due to their display of myriad exotic phenomena. Their electronic, structural and magnetic properties depend on a delicate energy balance and competition among spin states and various charge, orbital, and lattice degrees of freedom. For example, the complex behavior of the cobalt spin states effectively lead to the generation of superconductivity in $Na_xCoO_2 \cdot nH_2O$ [1], thermopower effects in stoichiometric $NaCo_2O_4$ [2], Li_xCoO_2 rechargeable batteries [3], ferromagnetism and electrical conductivity in $La_{1-x}Sr_xCoO_3$ [4], antiferromagnetism [5,6] as well as low-dimensional, disordered and/or frustrated magnetism in a number of Co-based compositions [7–10]. In turn, the recently discovered cobalt-rich $RBaCo_4O_{7+x}$ family "*R*-114" (*R* = Rare Earths or Y) has attracted interest because of the opportunity it provides to study many of the above-mentioned phenomena in one system. In particular, $RBaCo_4O_{7+\delta}$ materials have been shown to exhibit high affinity to oxygen, significant thermoelectric and transport properties, and frustrated magnetism [11–14].

In this family of *R*-114 materials, many members have been reported to crystallize in either the trigonal $P6_3mc$ [15,16] ($O_{7+\delta}$ materials; $0 \leqslant \delta < 0.2$) or orthorhombic $Cmc2_1$ (as in $ErBaZn_4O_{6.5}$ [17]) symmetries with the structures in both space groups sharing the same features and motifs but differing only by a subtle distortion of the oxygen sublattice due to the presence of the oxygen vacancies. The undistorted structure of $RBaCo_4O_7$ can be best described as a closely packed stack of alternating triangular (Co1 with *z*-coordinates ~0 and ~0.5) and Kagomé (Co2; *z*~0.25 and ~0.75) layers in which corner-sharing oxygen tetrahedra form with their centers occupied by Co^{2+}/Co^{3+} ions in the ratio of 3/1, respectively. Exactly

*Corresponding author at: Department of Physics, Northern Illinois University, DeKalb, IL 60115, USA.
E-mail address: chmaissem@anl.gov (O. Chmaissem).

0022-4596/$ - see front matter © 2008 Elsevier Inc. All rights reserved.
doi:10.1016/j.jssc.2007.12.016

half of the triangular units in the Kagomé plane are capped by Co1 ions to form columns running perpendicular to the Kagomé sheets. The *R* (or Y) and Ba cations occupy octahedral and anticuboctahedral sites, respectively, as shown in Fig. 1.

In a recent high-resolution neutron and synchrotron X-ray powder diffraction study [15], the structure of $YbBaCo_4O_7$ has been demonstrated to crystallize in a trigonal *P31c* symmetry at temperatures above 175 K. Evidence for the lower symmetry was found in the poor fit to the data when $P6_3mc$ was assumed, and in the anomalous thermal factors for Co2 and two of its oxygen first-neighbors. At temperatures below 175 K, a first-order structural phase transition to the orthorhombic $Pbn2_1$ symmetry has also been demonstrated. In this structure, significant distortion of the Co layers is observed in addition to the substantially distorted oxygen sublattice. The orthorhombic and hexagonal lattices are related through the relation $a_o = a_h$, $b_o = \sqrt{3}a_h$, $c_o = c_h$, where the subscripts "o" and "h" refer to orthorhombic and hexagonal, respectively. The authors suggest the origin of this first-order phase transition as a response to strongly underbonded Ba^{2+} ions and report no compelling evidence through bond valence sums for any Co^{2+}/Co^{3+} charge ordering involvement in this Yb-114 compound [15].

More recently, Chapon et al. [16] and Caignaert et al. [18] demonstrated that an Y-analog material, namely $YBaCo_4O_7$, exhibits structural features similar to $YbBaCo_4O_7$ albeit with the $P31c \rightarrow Pbn2_1$ structural phase transition occurring near room temperature, $T_S = 312$ K. A three-dimensional long-range antiferromagnetic order of the cobalt magnetic moments was observed below 110 K [16,19]. The threefold hexagonal symmetry of undistorted *R*-114 would cause its magnetic structure to be frustrated [14]. This frustration appears to be relieved by the observed structural phase transition and/or by increasing the material's oxygen content. Huq et al. [15] reported that the structure of their oxygen-rich $YBaCo_4O_{7.2}$ phase remains in the *P31c* symmetry down to 10 K and speculated that excess O may enhance the Ba–O bonding to the extent that the $P31c$–$Pbn2_1$ transformation is no longer favorable. They further speculated that the suppressed phase transition could lead to a frustrated magnetic state rather than long-range order. Thus, excess oxygen may explain the report of a magnetically frustrated state in the nominally stoichiometric $YBaCo_4O_7$ reported by Valldor [14] and Soda [19] and more recently in $Y_{0.5}Ca_{0.5}BaCo_4O_7$ [20].

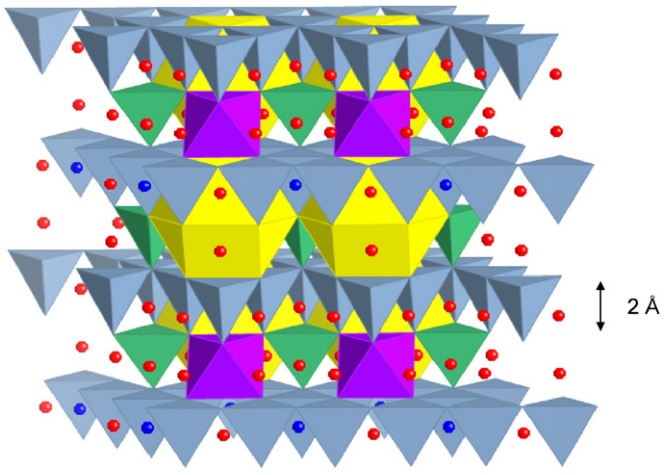

Fig. 1. The structure of $YBaCo_4O_7$ showing possible oxygen locations (blue and red circles) as suggested by Valldor et al. [14] and the separation distance of ~2 Å between the triangular and Kagomé layers (see text for details). Ba, Y, and Co polyhedra are shown as light-shaded (yellow) anticuboctahedra, dark-shaded (purple) octahedra, and medium-shaded (blue) tetrahedra, respectively.

The great affinity of $YBaCo_4O_7$ for oxygen has been firmly established by several research groups [21–24] who demonstrated the material's large oxidation–reduction capabilities at temperatures near 350 °C. As much as 1 to ~1.5 extra oxygen atoms per unit formula have successfully been added to the material at ambient and high oxygen pressures, respectively. Examining the closely packed trigonal structure of $YBaCo_4O_7$ reveals no "obvious" sites available for any additional oxygen, Fig. 1. Nonetheless, one can identify a significant distance between the adjacent Ba and Co2 Kagomé layers of ~2 Å from which extra oxygen atoms may potentially enter the structure and bond with the surrounding cations. The fixed oxidation states of the Y^{3+} and Ba^{2+} ions imply that the extra oxygen atoms must primarily bond with some of the cobalt ions to increase their average oxidation state from 2.25+ to 2.75+ (in $RBaCo_4O_8$). The increased number of oxygen first-neighbors and the well-known Co^{3+} chemistry [25] lead us to expect that some of the original tetrahedra would convert to pyramids or octahedra, or both.

In recent work, Valldor [14] identified three possible positions where the extra oxygen atoms might be incorporated. One of these sites is just under the Kagomé Co2 triangles and the remaining two sites are at the center of the Ba anticuboctahedra's square faces, Fig. 1. In the absence of significant structural distortions, the proposed positions would result in very short Ba–O (2.21 Å) and O–O (2.1–2.2 Å) bond lengths.

In this letter, we report the synthesis and structural determination of $YBaCo_4O_8$ in which the additional oxygen atoms order in a doubled superstructure unit cell, with respect to $Pbn2_1$, and cause considerable displacements of several of the original oxygen atoms. As a result of this controlled oxidation of $YBaCo_4O_7$, the coordination numbers for the various cations in the structure are significantly modified. The role of the extra oxygen is discussed in terms of its effects on the chemical environment, cationic oxidation states, and the material's solid-state chemistry and magnetic properties.

2. Experimental procedures

Single-phase $YBaCo_4O_{8.1}$ composition was prepared by the solid-state synthesis technique. Y_2O_3, $BaCO_3$, and

Co_3O_4 were mixed in stoichiometric ratios and heated at 1150 °C with several intermediate grindings, then cooled in air. The material was then annealed at 330 °C for 6 h in a flowing 20% O_2/N_2 mixture and quenched into liquid nitrogen. The oxygen content and high reproducibility of the final composition were confirmed by repeated thermogravimetric analyses. DC and AC magnetic susceptibilities were measured in a quantum design physical properties measurement system. For the DC measurements, data were collected after zero-field cooling (ZFC) or field cooling (FC) in 1 T. AC data were collected as a function of frequency after ZFC with an excitation field of 10 Oe. Full details of the synthesis and characterization will be published in a subsequent report.

Time-of-flight neutron powder diffraction data were collected at 300 and 10 K on the special environment powder diffractometer (SEPD) [26] at the intense pulsed neutron source (IPNS). High-resolution backscattering data, from 0.5 to 4 Å d-spacing, and medium resolution data, 1 to 10 Å d-spacing, were analyzed using the Rietveld method and the general structure analysis system (GSAS) code [27,28]. In the analysis, absorption, background, and peak width parameters were refined, together with the lattice parameters, atomic positions, and isotropic temperature factors.

High-resolution X-ray powder diffraction data were collected on beamline X16C at the National Synchrotron Light Source. A zero-background quartz plate was lightly coated with vacuum grease and a small amount of powdered sample was sprinkled onto it through a sieve. An X-ray powder diffraction pattern was collected over the 2θ angular range of 2–42°. The selected X-ray wavelength was 0.6965 Å, the sample was rocked 2° at each point, and the diffractometer was equipped with a Ge(1 1 1) analyzer crystal. The X-ray data were analyzed using TOPAS [29] for peak-indexing, determination of possible space groups, and joint structure refinement.

3. Results and discussion

3.1. Magnetic properties

The DC magnetic susceptibility (M/H) for $YBaCo_4O_{8.1}$ is shown in the main panel of Fig. 2. From 80 to 300 K, the data do not obey a Curie–Weiss relationship. At ~80 K, an inflection point can be seen, which is made clear in a plot of $d(M/H)/dT$, indicating the onset of weak ferromagnetism (FM). Isothermal magnetization measured near the peak at 60 K (not shown) evidences a large non-saturating component up to 9 T and an extremely small ferromagnetic hysteresis. A saturation moment at 50 K (where the loop is largest) of $4\times10^{-4}\,\mu_B$/Co can be crudely estimated by extrapolating the high-field linear regime to $H=0$. This is well below the detection limit of the powder neutron diffraction measurements discussed below. The divergence of FC and ZFC curves below ~60 K has been suggested by Tsipis et al. [22,30] to reflect glassiness in this oxygenated

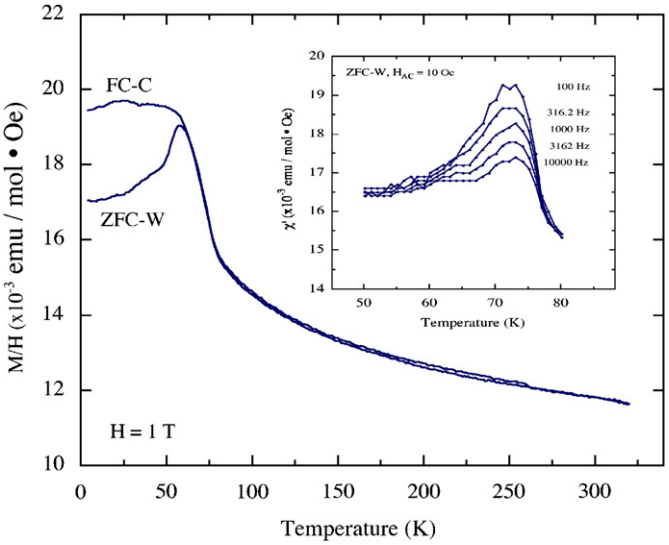

Fig. 2. Field Cooled (FC) and zero field cooled (ZFC) magnetization measurements for $YBaCo_4O_8$ showing very weak ferromagnetism below ~80 K (see text for more details). Inset: frequency-independent AC susceptibility measurements show that the material is not a spin glass.

Y-114 sample. However, the peak in the real part of the AC susceptibility (inset of Fig. 2) exhibits very little or no frequency dependence normally associated with spin-glass freezing. An alternative explanation is that the rapid (10 K/min) ZFC process freezes in a metastable high temperature phase that is non-ferromagnetic. Warming to ~60 K provides thermal activation nucleating the ferromagnetic phase, and the FC and ZFC curves merge. Indeed, isothermal magnetization data taken after rapid ZFC to 5 K are strictly linear. In this scenario, FC (at 2 K/min) does not bypass the first order phase transition, and the FM onset is observed at 80 K. Additional work will be required to verify this hypothesis and to fully understand the magnetic properties of this new compound.

3.2. Neutron and synchrotron X-ray diffraction and structural details

Initial examination of the neutron and synchrotron diffraction data for $YBaCo_4O_8$ revealed the unexpected presence of a large number of extra peaks (with respect to $YBaCo_4O_7$) as well as in significant peak splitting, Fig. 3. All peaks were unequivocally indexed to an orthorhombic superlattice of dimensions $a=12.790$ Å, $b=10.845$ Å, $c=10.149$ Å (i.e., $2a_o\times b_o\times c_o$ where the subscript "o" refers to the $Pbn2_1$ orthorhombic unit cell). Unsuccessful attempts to index the patterns using other hexagonal, orthorhombic, or monoclinic unit cells with different sizes provide convincing evidence of the cell uniqueness. Corroborating the X-ray data, the inset of Fig. 3(a) shows the (1 0 0) peak at ~12.79 Å observed in neutron diffraction at 300 K. Neutron data collected at 10 K (not shown) were similar to the 300 K dataset with no evidence observed for

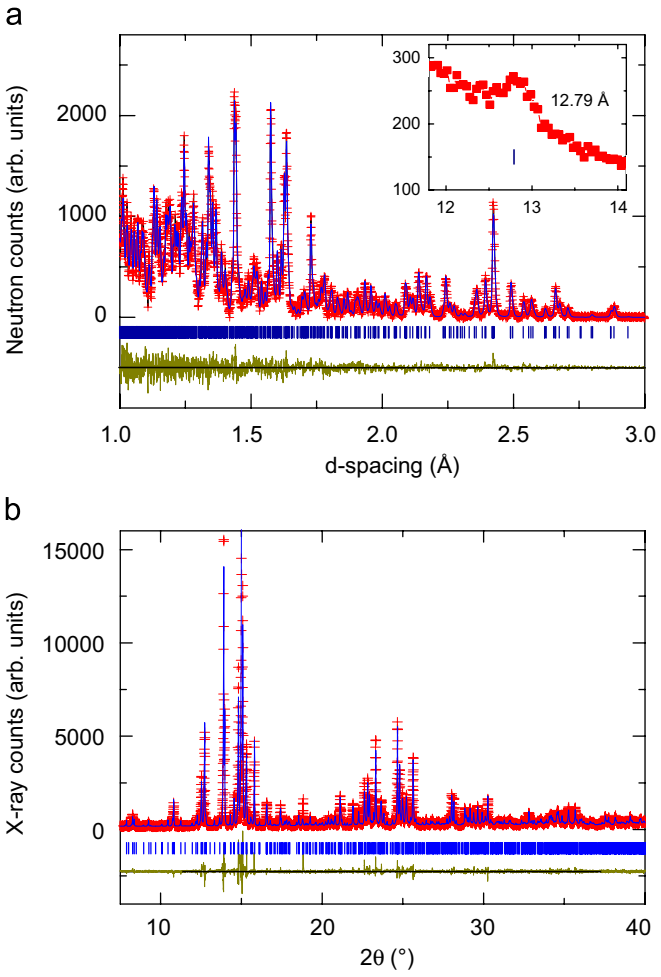

Fig. 3. Best-fit Rietveld refinement for $YBaCo_4O_8$ in the 1–3 Å d-spacing range (neutron data (a)) and $8^\circ \leqslant 2\theta \leqslant 40^\circ$ angular range (synchrotron data (b)) showing observed (plus signs) and calculated intensities (solid line) at 300 K. Background and incident spectrum have been subtracted. Tick marks below the pattern show the positions of the Bragg peaks. The difference between the observed and calculated intensities is displayed below the tick marks. Inset of (a): portion of the forward-scattering neutron data showing the (1 0 0) peak at 12.79 Å.

Table 1
Atomic structural parameters for $YBaCo_4O_8$

Name	X	Y	Z	B (Å^2)
Y1	0.3749(6)	0.0612(6)	0.4199(5)	1.5(2)
Y2	0.8604(6)	0.0951(6)	0.3871(8)	1.0(2)
Ba1	0.3758(4)	0.0728(4)	0.0275(6)	0.5(2)
Ba2	0.8966(4)	0.0763(5)	0	2.3(4)
Co11	0.375(1)	0.756(1)	0.461(1)	0.6(4)
Co12	0.125(1)	0.2569(9)	0.451(1)	0.3(4)
Co21	0.371(1)	0.5977(7)	0.212(1)	−0.9(3)
Co22	0.119(1)	0.0801(9)	0.207(1)	1.3(5)
Co23	0.2627(9)	0.333(1)	0.208(1)	1.0(6)
Co24	0.2291(8)	0.845(1)	0.214(1)	2.4(6)
Co25	0.4864(9)	0.318(1)	0.233(1)	0.9(4)
Co26	−0.0097(9)	0.843(1)	0.195(1)	1.2(5)
O1	0.295(1)	0.608(1)	0.049(2)	1.0(2)
O2	0.117(1)	0.079(1)	0.012(1)	0.7(2)
O3	0.249(2)	0.327(2)	0.022(2)	2.6(3)
O4	0.264(1)	0.852(1)	0.034(2)	1.8(3)
O5	0.538(1)	0.214(1)	0.117(2)	0.7(2)
O6	0.004(1)	0.827(1)	0.005(2)	1.3(2)
O7	0.447(1)	0.461(2)	0.140(2)	1.5(2)
O8	0.021(1)	0.513(2)	0.253(2)	2.0(3)
O9	0.104(1)	0.766(2)	0.276(2)	2.0(2)
O10	0.368(1)	0.233(2)	0.279(2)	2.0(2)
O11	0.138(1)	0.255(2)	0.262(2)	1.7(3)
O12	0.294(1)	0.719(2)	0.301(2)	1.7(2)
O13	0.268(1)	0.474(1)	0.292(2)	0.9(2)
O14	0.765(1)	0.504(1)	0.285(2)	−0.2(2)
O27	0.550(1)	0.384(1)	0.369(2)	−0.0(2)
O28	0.452(1)	0.616(2)	0.383(2)	2.4(3)

Refined lattice parameters are $a = 12.790(3)$ Å, $b = 10.845(2)$ Å, and $c = 10.149(2)$ Å; Cell volume = 1407.8(5) Å^3. The z-coordinate of the Ba2 position was fixed at 0. Agreement factors: $R_p = 2.43\%$, $R_{wp} = 3.35\%$, and $\chi^2 = 1.296$. Atomic site occupancies, refined to full occupancy within 1–3 standard deviations, were fixed at 1.0 in the final refinements.

any structural phase transition or long range antiferromagnetic ordering.

The numerous and relatively isolated peaks observed in the long d-spacing range of the neutron and X-rays patterns allowed for the extraction of extinction rules from which the choice of possible space groups was narrowed to $Pbc2_1$ (standard setting is $Pca2_1$). While there is no direct subgroup relationship with the established orthorhombic $Pbn2_1$ structure of $YBaCo_4O_7$, the doubling of the a-lattice parameter and near equality of the remaining parameters is highly suggestive of a close relationship of these structures. It is possible to fit an idealized O_7 structure into the doubled $Pbc2_1$ superlattice by a simple shift of origin. Additionally, $Pbc2_1$ could be related to the hypothetical parent $P6_3mc$ and $Cmc2_1$ space groups through the following sequence of group–subgroup relationship: $P6_3mc > Cmc2_1 > Pca2_1 > Pbc2_1$. A structural $Pbc2_1$ model results in a total of 26 independent atoms (all with site multiplicity of 4; $Z = 8$) in addition to the two extra oxygen positions that were determined in subsequent stages (Table 1).

Initial refinements of the structural model demonstrated that the Y, Ba, and Co sublattices remain similar to the parent $YBaCo_4O_7$ material. However, refinement of the oxygen locations quickly revealed the occurrence of significant displacements for a few oxygen atoms near several Co sites. The examination of these displacements allowed us to identify empty locations that the extra oxygen atoms could occupy. Further refinements of the oxygen positions and occupancies led to the conclusion that only two of the new positions are fully occupied, thus confirming the oxygen stoichiometry as O_8, while the occupancies of the remaining possible positions were essentially empty (within three standard deviations). However, the presence of the empty positions indicates that the structure may be viewed as an open network capable of absorbing still more oxygen in accord with reports of up to 0.5 additional O atoms [21–23].

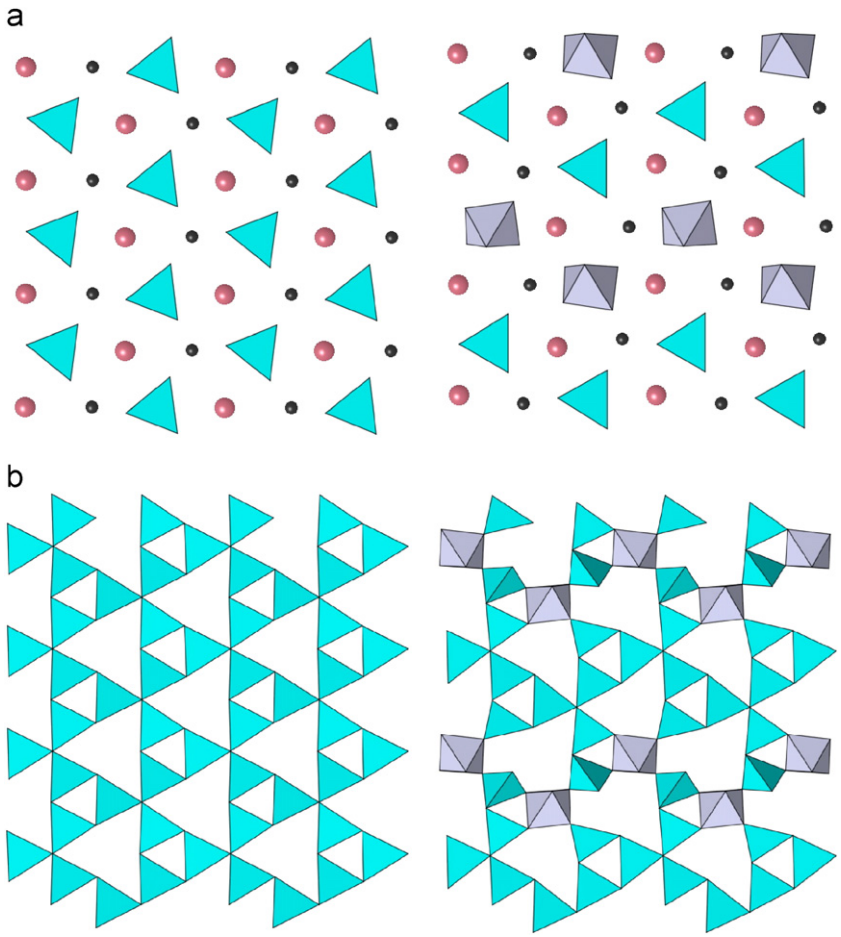

Fig. 4. Side-by-side views of the triangular (a) and Kagomé (b) layers for $YBaCo_4O_7$ (left) and $YBaCo_4O_8$ (right). Large red and small blue circles represent Ba and Y ions, respectively.

A side-by-side comparison of the first two triangular ($z\sim0$) and Kagomé layers ($z\sim0.25$) is displayed in Fig. 4 as they appear in the *Pbn2₁* ($YBaCo_4O_7$) and *Pbc2₁* ($YBaCo_4O_8$) structures. As shown in the figure, the extra oxygen atoms enter the structure to bond with half of the triangular cobalt ions and form zigzag patterns of Co1 octahedra. The resulting Co1 octahedra tilt around the *b*-axis, in an alternating sequence towards the positive and negative directions of the *a*-axis. The octahedra and remaining tetrahedra form alternating zigzag patterns that run parallel to each other along the *b*-axis.

In the "Kagomé" layer, Co2 octahedra form directly above and below the Co1-octahedra (in the $z\sim0$ and 0.5 layers, respectively) to form zigzag ribbons directed along the *c*-axis. In these chains, the edge-sharing octahedra tilt towards the positive or negative directions along and around the *a*- and *b*-axes, respectively, Fig. 4. A side-view [100] structural projection demonstrates the long-range zigzag ordering of the Co1 and Co2 octahedral chains, Fig. 5(a), and Kagomé-like distorted lattice planes at different *a*-values, Fig. 5(b). Here, it should be emphasized that the formation of zigzag chains of edge-sharing octahedra is extremely rare. Only recently, materials crystallizing with motifs that are close to ours have been identified as in $M_2P_4O_{12}$ and $M_2H_2P_2O_7$ ($M=$ Ni, Co) [31,32] and $BaY_2Si_3O_{10}$ [33], for example. However, we note that the structures of these materials are not "all oxide-like" structures with metal-O bonds (e.g., as in perovskites, spinels, etc.), but rather contain PO_4 or SiO_4 tetrahedra. To our knowledge, the present structure of $YBaCo_4O_8$ thus appears to be an extremely rare if not unique example of a mixed-metal oxide containing this structural motif.

Returning to the $z\sim0.25$ "Kagomé" layer, some of the original lattice remains largely unaffected; however, the immediate neighborhoods of the Co2 octahedra are significantly modified due to the presence of excess O sites. Due to the tilts around the *a*-axis, two of each octahedron's in-plane four corners shift significantly higher than the other atoms in the same layer, thereby pulling upward the two neighboring corner-shared Co tetrahedra and causing them to distort. The Co tetrahedra sharing the two remaining octahedron's in-plane corners are completely reoriented (with respect to those in the $YBaCo_4O_7$ structure). Fig. 6 shows a fragment of the structure in which corner-sharing Co tetrahedra/octahedra

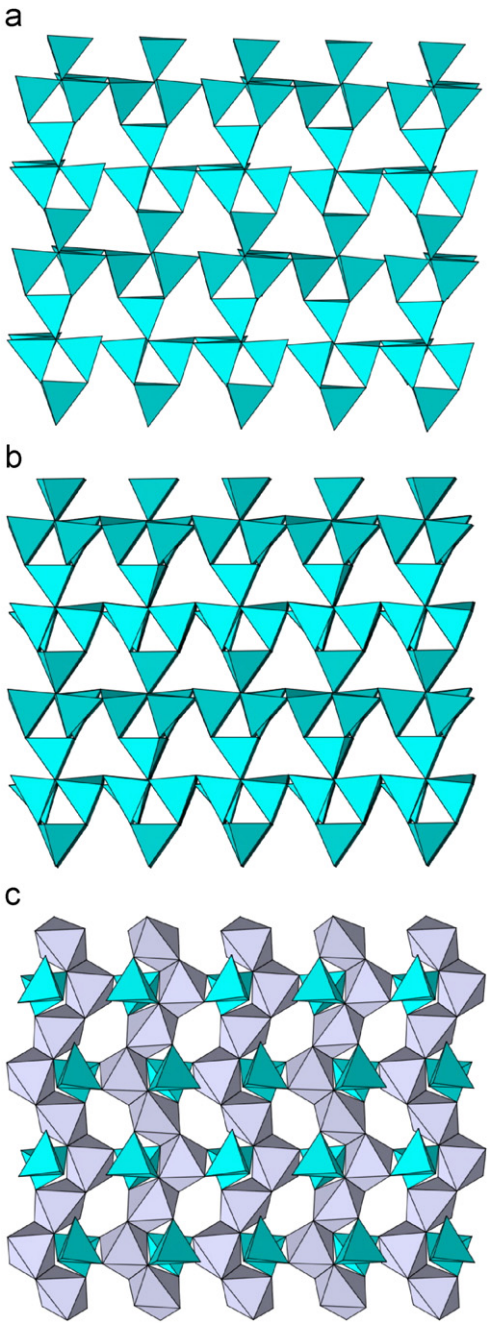

Fig. 5. Projection of the $YBaCo_4O_7$ (a) and $YBaCo_4O_8$ structures (b and c) along the [100] direction. The figure shows distorted Kagomé-like corner-sharing Co tetrahedra in both (a) and (b) and zigzag chains of edge-sharing Co octahedra directed along the *c*-axis in (c). The two $YBaCo_4O_8$ layers (b and c) are obtained at different *x*-values.

and edge-sharing octahedra/octahedra are emphasized as well as the locations of the new oxygen atoms.

In Fig. 7, we show a [010] projection of the structure in which the increased lattice distortions clearly result in significantly corrugated layers. This figure and the alternating octahedral/tetrahedral zigzag patterns (shown in Fig. 3) demonstrate the origin of the *a*-axis superlattice doubling.

In the $Pbn2_1$ structure of $YBaCo_4O_7$, the Y atoms occupy the centers of near-perfect oxygen octahedra. In contrast, there are two distinct Y sites in $Pbc2_1$ $YBaCo_4O_8$. In the first site, the Y ion remains at the center of a significantly distorted octahedron, but in the second site, the Y polyhedron is formed by one new oxygen atom along with the six original octahedral oxygen first-neighbors. All Y–O bond lengths are reasonable, falling in the range of 2.21–2.48 Å (Table 2).

The Ba polyhedra are significantly distorted with several of the oxygen atoms displaced away from or closer to Ba. As a result, two independent Ba sites are found with the Ba coordinated with 10 or 11 oxygen first neighbors. Most of the Ba–O bond lengths fall in the range of 2.7–3.3 Å, in addition to one short (2.53 Å) and one long bonds (3.5 Å), Table 2. It is worth noting that the significantly distorted Ba polyhedra and the fewer oxygen first neighbors make it difficult to compare our new oxygen positions with Valldor's predicted sites. However, none of our calculated Ba–O bond lengths is as short as Valldor's suggested Ba–O bonds [14], as the structure has significantly distorted with respect to the O_7 parent material.

Bond-valence sum (BVS) calculations ($v = \sum_i e^{(r_o - r_{ij})/B}$; see Ref. [34] for more details) show that the Y and Ba oxidation states are very close to their expected valences of 3+ and 2+, respectively, in both of their sites; see Table 2. Additionally, our calculations also suggest the oxidation states of 2+ or 3+ for the different cobalt sites, Table 2. As shown in Fig. 3, the zigzag stripe patterns in the "triangular" layers consist not only of alternating octahedra and tetrahedra but also of alternating charge ordered Co^{2+} and Co^{3+} ions. Thus, charge balance in the chemical formula suggests that each "Kagomé" layer would contain Co^{3+} and Co^{2+} ions, if charge ordered, in the ratio of 5 to 1, respectively. Instead, our BVS calculations (using r_o for Co^{2+} because of the lack of a reliable r_o value for Co^{3+}) show a ratio of $4Co^{3+}$ to $2Co^{2+}$. As expected, all octahedral Co are trivalent as are their surrounding first-neighbor tetrahedra. Bivalent corner-sharing Co tetrahedra form continuous zigzag ribbons in the *b*-axis direction, linking the chains of Co^{3+} polyhedra. We attribute the discrepancy between the calculated and the expected Co^{3+}/Co^{2+} ratio to arise from the fact that integral bond valence sums may be expected for simple and relaxed structures, which is certainly not the case in our material. In a series of recent publications, Brown [35,36] has recognized the importance of strain and structure complexity effects and reported the need for corrections to the nominal BVS formulation. Additional complications could come from possible orbital overlapping and hybridization between the concerned cations and their oxygen first neighbors. Indeed, in our $YBaCo_4O_8$ material, the clear distortions around some particular Co ions and the associated severe layer buckling (curvature) indicate the presence of significant tensile strains that could impact the BVS calculations. Nonetheless, it should be emphasized that the oxidation states for most of the independent cations (12 independent

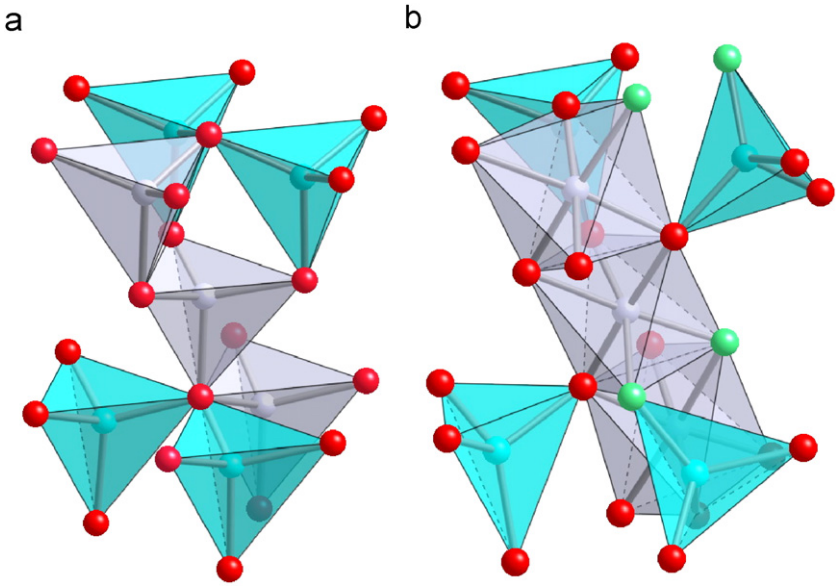

Fig. 6. Structural fragments for $YBaCo_4O_7$ (left) and $YBaCo_4O_8$ (right). The figure shows the drastic displacement of some oxygen atoms and the locations of the two new ones.

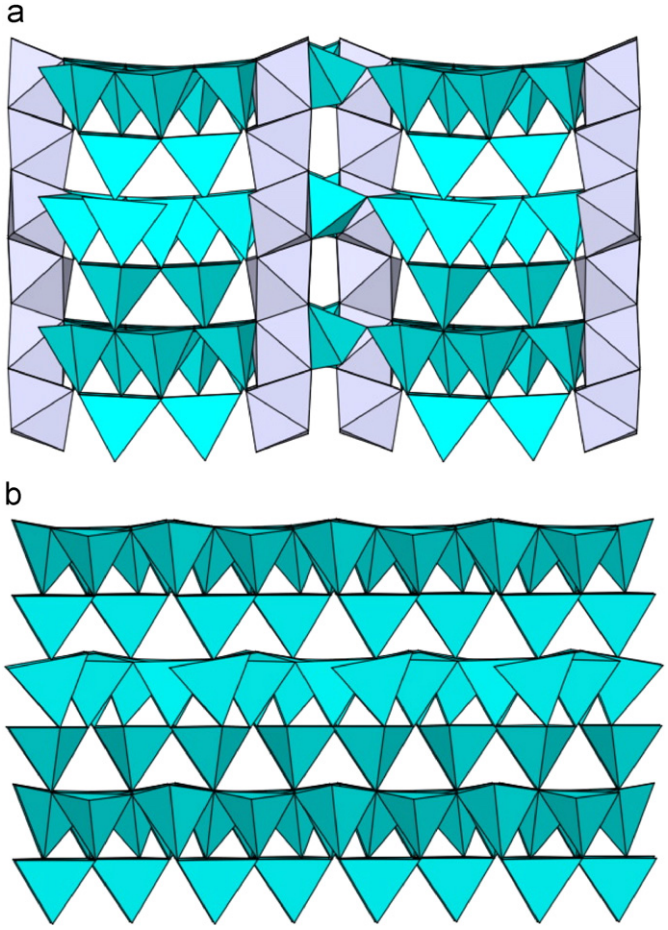

Fig. 7. Projection of the $YBaCo_4O_8$ structure along the [010] direction showing the material's structural distortions and corrugated layers (a). For comparison, a [010] projection of the $YBaCo_4O_7$ orthorhombic structure is also shown (b).

sites are present in this structure) are very reasonable, especially for Ba, when compared with those calculated for the parent $YBaCo_4O_7$ material.

Some of the tetrahedral Co^{3+}–O bond lengths are found to be significantly short (1.75–1.78 Å) compared with their tetrahedral Co^{2+}–O counterparts (1.87–2.02 Å). It is important to note here that the tetrahedral coordination for Co^{3+} is rare, and when found, the Co^{3+}–O bond lengths have been reported to be on the order of 1.78–1.79 Å [37,38]. This instability of tetrahedral Co^{3+} in the parent O_7 material evidently drives the strong affinity for oxygen uptake.

4. Conclusions

A huge unit cell volume of more than 1400 $Å^3$ together with 28 total independent sites attest to the originality of our $YBaCo_4O_8$ structure. As shown here, the extra oxygen atoms strongly break the threefold symmetry in all the layers and minimize the magnetic frustration. Hence, the loss of the triangular symmetry might be expected to facilitate long-range magnetic order as found in the parent $YBaCo_4O_7$ [16]. However, the neutron powder diffraction data collected at 10 K evidence no such long-range order. One could speculate that the Co^{3+} ions in octahedral coordination might adopt a low-spin configuration, effectively diluting the magnetic sublattice. Detailed work with theoretical guidance will be needed to fully understand this apparent contradiction.

Having determined this structure, certain questions now become inevitable: Should this structure be expected for other $RBaCo_4O_8$ structures regardless of the rare earth's ionic size? Is it still possible to fit more oxygen atoms in the

Table 2
Cation–oxygen bond lengths for all Ba, Y, and Co ions

Ba1–O2	3.3122(7)	Ba2–O1	2.5276(5)	Y1–O1	2.4780(3)	Y2–O2	2.2877(4)
Ba1–O3	3.1999(5)	Ba2–O2	2.8240(6)	Y1–O3	2.2670(3)	Y2–O4	2.2549(3)
Ba1–O4	2.7850(5)	Ba2–O3	3.2901(5)	Y1–O7	2.4324(4)	Y2–O6	2.2689(3)
Ba1–O5	2.7283(4)	Ba2–O6	3.0269(5)	Y1–O10	2.3428(4)	Y2–O8	2.2239(3)
Ba1–O7	2.8132(4)	Ba2–O6	3.0075(5)	Y1–O14	2.3363(3)	Y2–O9	2.2169(4)
Ba1–O10	3.0908(5)	Ba2–O8	2.8570(5)	Y1–O27	2.2091(4)	Y2–O13	2.3108(3)
Ba1–O10	3.2865(5)	Ba2–O8	3.1254(5)	Y1–O28	2.3207(5)		
Ba1–O13	2.8032(5)	Ba2–O9	3.4717(5)				
Ba1–O14	3.2583(5)	Ba2–O9	2.8487(4)				
Ba1–O27	2.7892(4)	Ba2–O14	2.8932(4)				
Ba1–O28	2.6952(4)						
v(Ba1)	2.03	v(Ba2)	1.86	v(Y1)	3.01	v(Y2)	3.14
Co11–O1	2.0064(3)	Co12–O2	1.8901(4)	Co21–O1	1.9241(3)	Co22–O2	1.9743(4)
Co11–O4	1.9835(3)	Co12–O3	1.9635(3)	Co21–O5	1.9669(3)	Co22–O8	1.9886(4)
Co11–O5	1.9665(3)	Co12–O6	1.9559(3)	Co21–O7	1.9128(3)	Co22–O11	1.9892(4)
Co11–O12	1.9708(3)	Co12–O11	1.9278(4)	Co21–O12	1.8845(2)	Co22–O14	1.8713(3)
Co11–O27	1.9239(3)			Co21–O13	2.0482(3)		
Co11–O28	1.9757(3)			Co21–O28	2.0268(3)		
v(Co11)	2.83	v(Co12)	2.08	v(Co21)	2.94	v(Co22)	1.98
Co23–O3	1.8960(4)	Co24–O4	1.8886(4)	Co25–O5	1.7540(2)	Co26–O6	1.9494(4)
Co23–O10	1.8814(3)	Co24–O9	1.9209(3)	Co25–O7	1.8869(3)	Co26–O8	1.9438(4)
Co23–O11	1.8913(3)	Co24–O12	1.8119(2)	Co25–O10	1.8328(3)	Co26–O9	1.8653(3)
Co23–O13	1.7583(3)	Co24–O14	1.8772(3)	Co25–O27	1.7596(3)	Co26–O11	2.0175(3)
v(Co23)	2.60	v(Co24)	2.46	v(Co25)	2.95	v(Co26)	2.05

The calculated oxidation states (v) are listed for each ion.

structure as suggested by the open frame network obtained from the refinements and by the reported $O_{8.5}$ compositions? The refined structure seems to indicate the presence of several additional locations where the bond lengths from oxygen to surrounding cations remain reasonable; however, the oxidation states of the different cations must be taken into consideration as they are expected to place an upper limit on how much extra oxygen can be incorporated.

Finally, the structure of $YBaCo_4O_8$ appears to suggest the possibility that creative chemical substitutions at the Co sites by non-magnetic ions may be used to isolate some Co ions in a one- or two-dimensional network of ordered chains; thus, possibly giving rise to controlled and reduced dimensionality of Co magnetic ordering.

In a recent XRD and XANES study, Valkeapää et al. [Chemistry Letters 36, 1368 (2007)] reported a similar unit cell for their $YBaCo_4O_{8.2}$ sample and an increased number of Co and O sites.

Acknowledgments

This work was partially supported by UChicago Argonne, LLC, Operator of Argonne National Laboratory. Argonne, a US Department of Energy Office of Science laboratory, is operated under Contract No. DE-AC02-06CH11357. Use of the National Synchrotron Light Source, Brookhaven National Laboratory, was supported by the US Department of Energy, Office of Basic Energy Sciences, under Contract No. DE-AC02-98CH10886. SNS is managed by UT-Battelle, LLC, under contract DE-AC05-00OR22725 for the US Department of Energy.

References

[1] K. Takada, H. Sakurai, E. Takayama-Muromachi, F. Izumi, R.A. Dilanian, T. Sasaki, Nature (London) 422 (2003) 53–55.
[2] I. Terasaki, Y. Sasago, K. Uchinokura, Phys. Rev. B 56 (1997) R12685–R12687.
[3] R.J. Gummow, M.M. Thackeray, W.I.F. David, S. Hull, Mater. Res. Bull. 27 (1992) 327–337.
[4] P. Ravindran, P.A. Korzhavyi, H. Fjellvag, A. Kjekshus, Phys. Rev. B 60 (1999) 16423–16434.
[5] J.R. Singer, Phys. Rev. 104 (1956) 929–932.
[6] T. Vogt, P.M. Woodward, P. Karen, B.A. Hunter, P. Henning, A.R. Moodenbaugh, Phys. Rev. Lett. 84 (2000) 2969–2972.
[7] H. Kageyama, K. Yoshimura, K. Kosuge, H. Mitamura, T. Goto, J. Phys. Soc. Jpn. 66 (1997) 1607–1610.
[8] Y. Yamaura, H.W. Zandbergen, K. Abe, R.J. Cava, J. Solid State Chem. 146 (1999) 96–102.
[9] R.J. Cava, A.P. Ramirez, Q. Huang, J.J. Krajewski, J. Solid State Chem. 140 (1998) 337–344.
[10] C. de Vaulx, M.-H. Julien, C. Berthier, S. Hebert, V. Pralong, A. Maignan, Phys. Rev. Lett. 98 (2007) 246402.
[11] D.V. Sheptyakov, A. Podlesnyak, S.N. Barilo, S.V. Shiryaev, D.D. Khalyavin, D.Yu. Chernyshov, N.I. Leonyuk, PSI Sci. Rep. 3 (2001) 64.
[12] M. Valldor, M. Andersson, Solid State Sci. 4 (2002) 923–931.
[13] M. Valldor, Solid State Sci. 6 (2004) 251–266.
[14] M. Valldor, in: J.V. Chang (Ed.), New Topics in Condensed Matter Research, Nova Science Publishers, New York, 2007, pp. 75–102.

[15] A. Huq, J.F. Mitchell, H. Zheng, L.C. Chapon, P.G. Radaelli, K.S. Knight, P.W. Stephens, J. Solid State Chem. 179 (2006) 1136–1145.
[16] L.C. Chapon, P.G. Radaelli, H. Zheng, J.F. Mitchell, Phys. Rev. B 74 (2006) 172401.
[17] C. Rabbow, H. Muller-Buschbaum, Z. Anorg. Alleg. Chem. 620 (1994) 527–530.
[18] V. Caignaert, A. Maignan, V. Pralong, S. Hebert, D. Pelloquin, Solid State Sci. 8 (2006) 1160–1163.
[19] M. Soda, Y. Yasui, T. Moyoshi, J. Phys. Soc. Jpn. 75 (2006) 054707.
[20] W. Schweika, M. Valldor, P. Lemmens, Phys. Rev. Lett. 98 (2007) 067201.
[21] M. Karppinen, H. Yamauchi, S. Otani, T. Fujita, T. Motohashi, Y.-H. Huang, M. Valkeapaa, H. Fjellvag, Chem. Mater. 18 (2006) 490–494.
[22] E.V. Tsipis, D.D. Khalyavin, S.V. Shiryaev, K.S. Redkina, P. Nunez, Mater. Chem. Phys. 92 (2005) 33–38.
[23] H.S. Hao, J.H. Cui, C.Q. Chen, L.J. Pan, J. Hu, X. Hu, Solid State Ionics 177 (2006) 631–637.
[24] A. Maignan, V. Caignaert, D. Pelloquin, S. Hebert, V. Pralong, Phys. Rev. B 74 (2006) 165110.
[25] A.F. Wells, Structural Inorganic Chemistry, 5th ed, Oxford University Press, New York, 1984.
[26] J.D. Jorgensen, J.J. Faber, J.M. Carpenter, R.K. Crawford, J.R. Haumann, R.L. Hitterman, R. Kleb, G.E. Ostrowski, F.J. Rotella, T.G. Worlton, J. Appl. Crystallogr. 22 (1989) 321–333.
[27] A.C. Larson, R.B. von Dreele, General Structure Analysis System (GSAS), Los Alamos National Laboratory Report LAUR 86748, 2000.
[28] B.H. Toby, J. Appl. Crystallogr. 34 (2001) 210–213.
[29] Bruker AXS (2005), TOPAS V3: general profile and structure analysis software for powder diffraction data, User's Manual, Bruker AXS, Karlsruhe, Germany; TOPAS, Academic is available at: ⟨http://pws.prserv.net/Alan.Coelho⟩.
[30] E.V. Tsipis, V.V. Kharton, J.R. Frade, P. Nunez, J. Solid State Electrochem. 9 (2005) 547–557.
[31] A. Olbertz, D. Stachel, I. Svoboda, H. Fuess, Z. Kristallogr. New Cryst. Struct. 213 (1998) 241–242.
[32] T. Yang, J. Ju, G.B. Li, S.H. Yang, J.L. Sun, F.H. Liao, J.H. Lin, J. Sasaki, N. Toyota, Inorg. Chem. 46 (2007) 2342–2344.
[33] U. Kolitsch, M. Wierbicka, E. Tillmanns, Acta Crystallogr. C 62 (2006) I97–I99.
[34] I.D. Brown, D. Altermatt, Acta Crystallogr. B 41 (1985) 244–247.
[35] I.D. Brown, J. Solid State Chem. 82 (1989) 122–131.
[36] I.D. Brown, J. Solid State Chem. 90 (1991) 155–167.
[37] G. Muncaster, G. Sankar, C. Richard, A. Catlow, J.M. Thomas, S.J. Coles, M. Hursthouse, Chem. Mater. 12 (2000) 16–17.
[38] A.M. Beale, G. Sankar, C. Richard, A. Catlow, P.A. Anderson, T.L. Green, Phys. Chem. Chem. Phys. 7 (2005) 1856–1860.